parafac4microbiome: Exploratory analysis of longitudinal microbiome data using Parallel Factor Analysis

G.R. van der Ploeg[1], J.A. Westerhuis[1*], A. Heintz-Buschart[1], A.K. Smilde[1]

[1] *Biosystems Data Analysis, Swammerdam Institute for Life Sciences, University of Amsterdam, Amsterdam, The Netherlands*

*Author for correspondence: Johan Westerhuis j.a.westerhuis@uva.nl

Geert Roelof van der Ploeg: https://orcid.org/0009-0007-5204-3386

Johan Westerhuis: https://orcid.org/0000-0002-6747-9779

Anna Heintz-Buschart: https://orcid.org/0000-0002-9780-1933

Age Smilde: https://orcid.org/0000-0002-3052-4644

Abstract

Background: Recently, studies that investigate microbial temporal dynamics have become more frequent. In a longitudinal microbiome study design, microbial abundance data are collected across multiple time points from the same subjects. In this context, exploratory analysis of longitudinal microbiome data using Principal Component Analysis is insufficient because the study design is not fully utilized. Indeed, the study design can be used to create a three-way data array where the rows constitute the subjects, the columns contain the microbial abundances, and the third dimension contains the time points. Organising the data this way enables multi-way methodologies that take full advantage of the study design. In this work we present Parallel Factor Analysis (PARAFAC) as a method to explore longitudinal microbiome data using three exemplary studies.

Results: In the first example study, a long time series of experimental in vitro microbiomes, we show that PARAFAC can identify the main time-resolved variation in longitudinal microbiome data. In the second example, a longitudinal infant gut microbiome study, we show that PARAFAC can find differences between subject groups and enhance comparative analysis despite a moderate amount of missing data. In the third example, a longitudinal gingivitis intervention study of the oral

microbiome, we show that PARAFAC helps identify microbial groups of interest using a post-hoc clustering approach.

Conclusions: We show that Parallel Factor Analysis is an applicable method for longitudinal microbiome data analysis across a wide range of microbial environments. The analyses and the example datasets with the resulting figures are implemented in the R package `parafac4microbiome`, which is available on CRAN at https://cran.rstudio.com/web/packages/parafac4microbiome/.

Key Words

Multi-way, PARAFAC, Tensor Factorization, Decomposition, Dynamics

Background

The role of the microbiome in biological systems and in disease has been thoroughly explored [1–3]. However, most studies are cross-sectional while microbial temporal dynamics are required to understand host-microbiome and microbe-microbe interactions [4, 5]. Recently, studies that investigate these dynamics have become more frequent [6–8].

In a longitudinal microbiome study design, microbial abundance data are collected across multiple time points from the same subjects [9–11]. These data are often stored in a two-way data table, where the rows constitute the measurements (samples from multiple individuals over time), and the columns contain the microbial abundances (**Figure 1A**). Two-way ordination methods like Principal Component Analysis [12, 13] are then employed to explore the data (**Figure 1B**). However, this often results in hard-to-interpret visualizations because these methods treat every measurement as a separate object to be ordinated (**Figure 1D, E**). As such, there is a need for exploratory methods that take the crossed longitudinal study design into account.

The longitudinal study design can be used to create a three-way data array where the rows constitute the subjects, the columns contain the microbial abundances, and the third dimension contains the time points (**Figure 1A**). Three-way ordination methods like Parallel Factor Analysis (PARAFAC; [14, 15]) can then be used to explore the data (**Figure 1C**). By making full use of the study design, the model can identify subject groups as well as their time profiles (**Figure 1D, F**).

In this work we present Parallel Factor Analysis as a method to explore longitudinal microbiome data. We first give a mathematical description of the PARAFAC method and its main requirement,

58 followed by a brief review of longitudinal microbiome data processing needed to meet this
59 requirement and the principles of PARAFAC model selection. We then highlight the benefits of
60 making a PARAFAC model using three exemplary datasets. In the first example study [6] we
61 highlight the time-resolved variation that PARAFAC models. In the second study [7], we highlight
62 how PARAFAC can find differences between subject groups and enhance comparative analysis
63 despite a moderate amount of missing data. In the third study [8] we highlight a post-hoc clustering
64 approach to identify microbes of interest with PARAFAC. The analyses and the example datasets
65 with the resulting figures are implemented in the R package `parafac4microbiome`, which is
66 available on CRAN at https://cran.rstudio.com/web/packages/parafac4microbiome/.

67

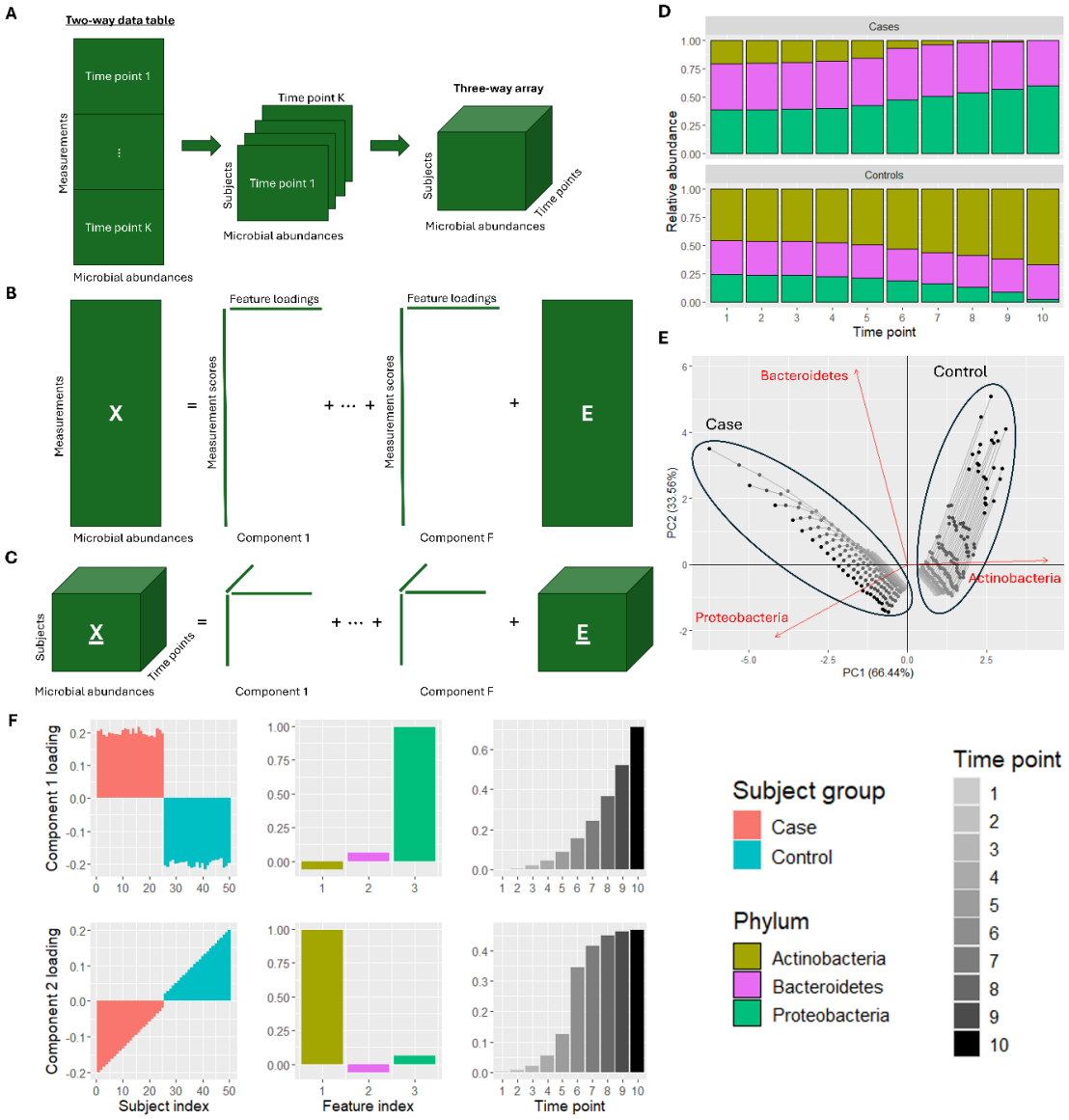

Figure 1: (A) Longitudinal microbiome data is often presented as a two-way data table with measurements (i.e. one sample for every subject-time point combination) in the rows and microbial abundances in the columns. This kind of data can be converted to a three-way array by putting all measurements for each time point in the third dimension. (B) Principal Component Analysis decomposes a two-way data table into components with scores for the measurements and loadings for the microbial relative abundances. This does not take the longitudinal study design into account. (C) Parallel factor analysis decomposes a three-way data array into components with three loading vectors each: one for the subjects, one for the microbial relative abundances, and one for time. (D) In a mock intervention dataset, we have obtained count data of three phyla (Actinobacteria, Bacteroidetes and Proteobacteria) corresponding to 25 case and 25 control subjects across 10 time points. At time point 1, all subjects look very similar to each other. At time point 10 the case subjects are depleted of Actinobacteria and enriched in Proteobacteria, while for the control subjects the opposite is true. The depletion and enrichment of the Actinobacteria at time point 10 varies substantially within the case and control groups, respectively. The simulated counts corresponding to Bacteroidetes have no time-resolved subject group differences. (E) Biplot of a Principal Component Analysis of the mock dataset after centred log-ratio transformation, centring and scaling. Samples taken from the same subject are connected with a line. The first principal component, explaining 66.44% of the variation, separates the case and control samples based on the abundance of Actinobacteria. The second principal component, explaining 33.56% of the variation, separates the time points using the Proteobacteria and Bacteroidetes abundances. However, the time profiles per subject group are unclear. (F) Plot of the Parallel Factor Analysis model of the data, describing subject group differences and their time profiles. In component 1 the exponential growth of Proteobacteria in the case subjects is identified. In component 2 the sigmoid shaped growth curve of Actinobacteria in the control subjects is identified. Bacteroidetes has a loading close to zero in both components, correctly identifying it as having no discriminating time-resolved variation. This illustrates that PARAFAC can capture various time-resolved differences in microbial abundances between the subject groups in a more interpretable way than PCA.

Methods

Notation and definitions

We briefly define the mathematical notation that will be used throughout this paper. Scalars are indicated by lower-case italics such as a. Vectors are indicated by bold lower-case characters such as $\boldsymbol{b}$. Two-way matrices are indicated with bold capitalized characters such as $\boldsymbol{X}$. Underlined bold capitalized characters are used for three-way arrays such as $\underline{\boldsymbol{X}}$. The letters I, J, and K are reserved to indicate the dimension of the subject, microbial abundance, and time mode, respectively. Hence the element for subject $i \in (1 \dots I)$, microbial abundance $j \in (1 \dots J)$ at timepoint $k \in (1 \dots K)$ of a three-way array $\underline{\boldsymbol{X}}$ is called x_{ijk}. We create the data cubes of microbial relative abundances such that the subjects are in the first mode, the microbial taxa are in the second mode, and time points are in the third mode. We will not distinguish between the terms 'factor' and 'component', nor between the terms 'way' and 'mode'. Generally, we will use the words 'component' and 'mode' throughout this paper.

Mathematical definition of Parallel Factor Analysis

Parallel Factor Analysis (PARAFAC) [14, 15] is a factor decomposition method that generalizes Principal Component Analysis (PCA) to multi-way. First, we give a brief mathematical summary of PCA to make the generalizing principle of PARAFAC clearer. We then describe the algorithmic implementation of this method and its properties.

A longitudinal microbiome dataset is often represented as a two-way matrix $\boldsymbol{X}$ $(IK \times J)$ with all time points for all subjects as rows and the microbial abundances as columns (**Figure 1B**). For convenience, we will refer to a subject-timepoint combination as a measurement $m \in (1 \dots M)$ where $M = IK$. A PCA model of this two-way dataset $\boldsymbol{X}$ $(M \times J)$ is then given by the two matrices $\boldsymbol{T}$ $(M \times F)$ and $\boldsymbol{P}$ $(J \times F)$ containing the scores and loadings of all F components respectively. The scores describe the differences between the measurements, and the loadings describe the microbial abundances that are different. A PCA model of such a two-way matrix can be formulated elementwise as

$$x_{mj} = \sum_{f=1}^{F} t_{mf} p_{jf} + e_{mj} \tag{1}$$

with x_{mj} the matrix element corresponding to measurement m and feature j, t_{mf} the score of measurement m in component f, p_{jf} the loading of feature j in component f and e_{mj} the residual of the matrix element. PCA is a bilinear model as we are using F sets of two vectors to approximate the dataset $\boldsymbol{X}$. This also reveals the main issue at hand: the measurements M are ordinated without taking the connection to the subjects I and time points K into account.

A three-way data array $\underline{\boldsymbol{X}}$ is defined as having I subjects in the rows, J microbial abundances in the columns and K time points in the third dimension (**Figure 1C**). A PARAFAC model of a three-way data array $\underline{\boldsymbol{X}}$ $(I \times J \times K)$ is given by three matrices $\boldsymbol{A}$ $(I \times F)$, $\boldsymbol{B}$ $(J \times F)$ and $\boldsymbol{C}$ $(K \times F)$ containing the loadings of all F components corresponding to the subject, feature, and time mode, respectively. The element-wise definition of the model is formulated as

$$x_{ijk} = \sum_{f=1}^{F} a_{if} b_{jf} c_{kf} + e_{ijk} \tag{2}$$

with x_{ijk} the matrix element corresponding to subject i, feature j at time point k, a_{if} the loading of subject i of component f, b_{jf} the loading of feature j of component f and c_{kf} the loading of time point k of component f and e_{ijk} the residual of the matrix element. In the elementwise definition, the generalization of PCA is readily visible: the loading for the time mode c_{kf} has been added to the calculation of element x_{ijk} to represent the time factor. PARAFAC is a trilinear model as we are using F sets of three vectors to approximate the data array $\boldsymbol{X}$.

Algorithmic implementation of Parallel Factor Analysis

The objective of the algorithmic implementation of PARAFAC is to minimise the sum-of-squares of the residuals through the loss function

$$L(a_{11}, a_{12}, \dots, c_{KF}) = \sum_{i=1}^{I} \sum_{j=1}^{J} \sum_{k=1}^{K} \left(x_{ijk} - \sum_{f=1}^{F} a_{if} b_{jf} c_{kf} \right)^2 \tag{3}$$

Various implementations of estimating the PARAFAC loading matrices exist [16]. In this paper we estimate the PARAFAC loading matrices through an iterative alternating least-squares algorithm (ALS; [15, 17]), as this implementation is well-documented and robust towards missing values or time points (**Table 1**).

Table 1: Algorithmic implementation of the alternating least squares based PARAFAC model estimation.

Parallel Factor Analysis (PARAFAC) ALS algorithm for a given three-way array $\underline{\boldsymbol{X}}$
(0) Decide on the number of components F
(1) Initialise $\boldsymbol{B}$ and $\boldsymbol{C}$
(2) Estimate $\boldsymbol{A}$ from $\underline{\boldsymbol{X}}, \boldsymbol{B}$ and $\boldsymbol{C}$ such that $L(a_{11}, a_{12}, \dots, c_{KF})$ is minimised
(3) Estimate $\boldsymbol{B}$ from $\underline{\boldsymbol{X}}, \boldsymbol{A}$ and $\boldsymbol{C}$ such that $L(a_{11}, a_{12}, \dots, c_{KF})$ is minimised
(4) Estimate $\boldsymbol{C}$ from $\underline{\boldsymbol{X}}, \boldsymbol{A}$ and $\boldsymbol{B}$ such that $L(a_{11}, a_{12}, \dots, c_{KF})$ is minimised
(5) Continue to step (2) until convergence.

Various approaches for initialisation of $\boldsymbol{B}$ and $\boldsymbol{C}$ have been proposed and are documented elsewhere [18]. In this paper, we used randomly initialised vectors to determine the appropriate number of components and singular value decomposition-based initialised vectors to investigate the stability of the loadings.

We use the PARAFAC algorithm supplied in the `parafac4microbiome` R package (v1.0.3[19]). With our default settings, the model is converged in step (5) when the change in sum-of-squares is lower than 1e-4 or after 500 iterations of steps 2-4. Fitting a model for any of the processed datasets in this paper takes less than a minute of computational time on an average computer (Microsoft Windows 11 Home v10.0.22631 with an 12th Gen Intel® Core™ i5-12400F running 2500 MHz with 6 cores or 12 logical processors and 16 Gb RAM).

PARAFAC model constraints and properties

A PARAFAC decomposition is unique, meaning that the estimated component matrices cannot be rotated without a loss of fit. This is a distinct advantage over Principal Component Analysis [15, 20–23]. Additionally, PARAFAC can capture any type of temporal dynamics – linear, exponential or otherwise - because it models time categorically. Thus, the time points are not connected like in a dynamic model. A limitation of PARAFAC is that all subjects must be measured on the same time points. While the method cannot interpolate or extrapolate to time points that were not originally measured, it can interpolate data that is missing in some subjects. Furthermore, the components are orthogonal in PCA while in PARAFAC the components are non-orthogonal by default. The orthogonality constraint in PCA results in models that force interpretation in terms of orthogonal factors which do not always align with the underlying biology, whereas the absence of such a constraint for PARAFAC results in models that can describe processes that are not necessarily

169 independent. Non-orthogonality is an advantage because it is more likely a realistic representation
170 of the biological system of interest. The downside of non-orthogonality is that components can be
171 very similar to each other. As such, interpretation should be done with care: examining one
172 component at a time can lead to wrong conclusions and plotting the loadings of two components
173 against each other requires a transformation (**Supplementary Methods**). Possible additional
174 constraints such as orthogonality and non-negativity of the loadings are described elsewhere [18,
175 19]. In this paper we will not constrain the PARAFAC models.

176 *Processing of longitudinal microbiome data*

177 The main requirement of PARAFAC is that the residuals are distributed symmetrically around zero
178 [14, 15, 18]. In this paper we perform the following four processing steps for each dataset to meet
179 this requirement: centred log-ratio transformation, feature filtering, centring and scaling. In this
180 section we outline these operations for multi-way data arrays (**Figure 2**). In the supplied R package,
181 the function processDataCube() performs each of these steps according to user specifications.

182 Centred log-ratio transformation (CLR) is a popular method to create a version of the data that can
183 be ordinated and interpreted through Euclidean distances [24]. This transformation approach deals
184 with the compositionality inherent to microbiome data and makes the data quantitative [25].
185 However, it is hampered by the zero-inflation commonly observed in microbiome data because
186 zeroes are not defined in log space [26]. Here we choose to CLR transform the datasets after adding
187 a pseudo-count of 1 to all counts (hereafter $\underline{\boldsymbol{X}^{clr}}$), which appears to yield similar models as other
188 pseudo-count strategies based on a brief sensitivity analysis (**Supplementary Figure 18**).

189 Due to the high dimensionality of the microbiome data, filtering of the features is a requirement to
190 model the data appropriately and quickly [27, 28]. However, in longitudinal microbiome data the
191 complete time trajectory of a feature should be considered prior to filtering. As such, we define the
192 sparsity of a feature as the fraction of measurements where the feature has zero counts. A sparsity
193 threshold can then be established to select features that are common, thus controlling the number
194 of zeroes in the data. Sparsity-based feature filtering is based on the count data and is applied after
195 the centred log-ratio transformation step. Since sparsity filtering is heavily dependent on the
196 sequencing depth and microbiome complexity, no overall sparsity threshold can be suggested here.
197 Therefore, a manual inspection of the sparsity per feature histogram is required to find a good

balance between removing too many features and keeping features with enough variation of interest. The calculateSparsity() function in the supplied R package can be used for this purpose.

After CLR transformation and feature filtering, we used centring to remove offsets in the data [29, 30]. This can be done in three different directions for three-way arrays: across the subject mode, across the feature mode and across the time mode. Centring across the subject mode removes the average subject time profile from every combination of microbial abundance and time point, i.e.

$$x_{ijk}^{cnt} = x_{ijk} - \frac{\sum_{i=1}^{I} x_{ijk}^{clr}}{I}. \tag{4}$$

Centring across the feature mode removes the average feature time profile from every combination of subject and time point, i.e.

$$x_{ijk}^{cnt} = x_{ijk} - \frac{\sum_{j=1}^{J} x_{ijk}^{clr}}{J}. \tag{5}$$

Centring across the time mode removes the average overall time profile from every combination of subject and microbial abundance, i.e.

$$x_{ijk}^{cnt} = x_{ijk} - \frac{\sum_{k=1}^{K} x_{ijk}^{clr}}{K}. \tag{6}$$

Here x_{ijk}^{cnt} refers to the centred value of the ijk-th element in the data cube across the various directions specified above, and x_{ijk}^{clr} refers to the CLR transformed value of the ijk-th element. Both centring across the subject mode and across the feature mode affects the interpretation of the time mode as deviations from the average profile will be modelled. Since we expect individual offsets to be present in the exemplary studies and wish to focus on differences between the individuals, we centre across the subject mode. As a result, the PARAFAC models will describe deviations from the average time profile.

After centring, we scaled the data to change the importance attached to different parts [29, 30]. For three-way arrays, this involves scaling a two-way matrix to standard deviation one. As such, there are two possibilities for three-way arrays: scaling within the subject mode and scaling within the feature mode. Scaling within the subject mode makes the standard deviation for all counts across all subjects and microbial abundances per time point equal to one, i.e.

$$x_{ijk}^{scl} = \frac{x_{ijk}^{cnt}}{\sqrt{\sum_{j=1}^{J}\sum_{k=1}^{K}\frac{\left(x_{ijk}^{cnt}\right)^2}{JK}}} \,. \tag{7}$$

This makes all time points equally important for the modelling procedure. Scaling within the feature mode makes the standard deviation across all subjects and time points per microbial abundance equal to one, i.e.

$$x_{ijk}^{scl} = \frac{x_{ijk}^{cnt}}{\sqrt{\sum_{i=1}^{I}\sum_{k=1}^{K}\frac{\left(x_{ijk}^{cnt}\right)^2}{IK}}} \,. \tag{8}$$

Here x_{ijk}^{scl} refers to the scaled value of the ijk-th element in the data cube within the various directions specified above and x_{ijk}^{cnt} refers to the CLR transformed and centred value of the ijk-th element in the data cube. This makes all microbial abundances equally important for the modelling procedure. Since we are interested in groups of microbiota with different time profiles, we scale within the feature mode. The processing steps used for all datasets in this paper are outlined in **Figure 2**.

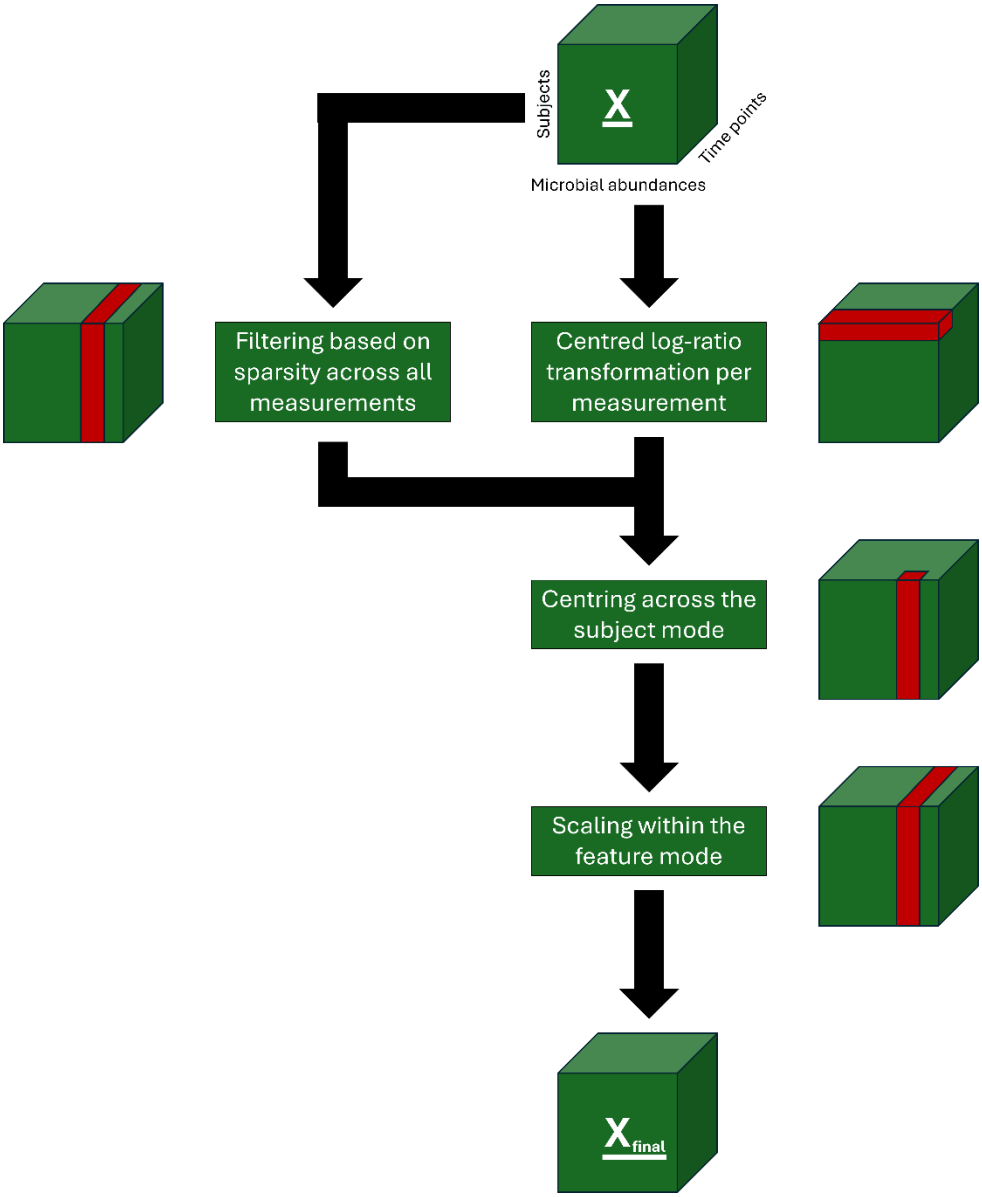

Figure 2: Workflow diagram of steps taken to process the microbiome count data for each dataset presented in this paper. The microbiome count data is indicated as $\underline{X}$ at the top of the figure. Per step, a small figure of the data cube is shown with the part of the cube that is used for the operation indicated in red. Sparsity-based feature filtering is based on the count data and is applied after the centred log-ratio transformation step. The final version of the data that is used as input for the PARAFAC modelling procedure is indicated as $\underline{X}_{final}$ at the bottom of the figure.

Example dataset: Fujita et al., 2023

The first example is a long time series of experimental in vitro microbiomes [6]. Culture conditions, microbiome sampling, 16S rRNA gene amplicon sequencing and data pre-processing are described in the original publication. We analyse only one experimental set-up, the aquatic microbiome culture in a peptone medium, which was performed in eight replicates and measured daily for 110 days.

246 The amplicon sequence variant (ASV) data and taxonomic information were processed using the
247 `parafac4microbiome` package (v1.0.3) in R (v4.4.1; [31]). The supplied dataset is a three-way array
248 of counts of size 8 replicates x 28 microbial (ASV) abundances x 110 time points. Features were kept
249 if they had ≤99% sparsity across the dataset (**Supplementary Figure 1**). This step resulted in 23
250 features being selected. We performed a centred log-ratio transformation with a pseudo-count of 1
251 to correct for compositionality [24, 25]. The data was then centred across the subject (here: replicate)
252 mode and scaled within the feature mode. PARAFAC models of the processed data were created
253 with convergence parameters set to ctol=1e-6 and maxit=500 to produce high-confidence solutions.

254 *Example dataset: Shao et al., 2019*

255 The second example is a longitudinal faecal microbiome study with samples collected from 314
256 vaginally born and 282 caesarean-section born infants [7]. Sampling was performed at four time
257 points after birth: day 4, 7, 21, and a follow-up sample was taken between 4 to 12 months (referred
258 to as the infancy period). Recruitment, microbiome sampling and 16S rRNA gene amplicon
259 sequencing and pre-processing are described in the original publication.

260 Pre-processed sequencing data were obtained from ENA (accession numbers ERP115334 and
261 ERP024601). Taxonomic classification was performed using mOTUs (v2.5.1; [32]). The marker-
262 gene based operational taxonomic unit (mOTU) data and taxonomic information were processed
263 using the `parafac4microbiome` package (v1.0.3) in R (v4.4.1; [31]). The supplied dataset is a three-
264 way array of counts of size 395 subjects x 959 microbial (mOTU) abundances x 4 time points, keeping
265 missing measurements as a row of NAs. This allows PARAFAC to impute the missing values. In
266 total, 62.5% of the data was missing (**Supplementary Tables 1-2**). mOTUs were kept if the sparsity
267 in either birth mode group was ≤90% (**Supplementary Figure 5**). This conserves biologically relevant
268 mOTUs that only appear in one group and resulted in 91 of the 959 mOTUs being selected. The data
269 was then centred log-ratio transformed using a pseudo-count of 1 to correct for compositionality
270 [24, 25]. Subsequently, the data was centred across the subject mode and scaled within the feature
271 mode. PARAFAC models of the processed data were created with convergence parameters set to
272 ctol=1e-8 and maxit=500 to produce high-confidence solutions given the large amount of missing
273 data.

274 *Example dataset: Van der Ploeg et al., 2024*

The third example is a longitudinal oral microbiome gingivitis intervention study [8]. Full details on the microbiome sampling and pre-processing are described in the original publication. We analyse only one oral microbiome niche, the supragingival plaque at the upper jaw lingual surfaces, which was measured in 41 subjects at 7 time points: day -14 (baseline), 0 (baseline, start of intervention), 2, 5, 9, 14 (end of intervention) and 21 (resolution). Using quantitative light-induced fluorescence [33–35], the subjects were stratified into low, medium and high responders based on the amount of red fluorescent plaque on day 14.

The ASV data and taxonomic information were processed using the `parafac4microbiome` package (v1.0.3) in R (v4.4.1; [31]). The supplied dataset is a three-way array of counts of size 41 subjects x 2253 microbial (ASV) abundances x 7 time points. In accordance with the original analysis, ASVs were kept if the sparsity was ≤50% in any response group. This step resulted in 65 of the 2253 ASVs being selected. Subsequently, a centred-log ratio transformation using a pseudo-count of 1 was performed to correct for compositionality [24, 25]. The data was then centred across the subject mode and scaled within the feature mode. PARAFAC models of the processed data were created with convergence parameters set to ctol=1e-6 and maxit=500 to produce high-confidence solutions.

Selecting the appropriate number of PARAFAC components

Like in Principal Component Analysis, the number of biologically meaningful components that can be extracted from longitudinal microbiome data is limited. After a given number of components, PARAFAC will start to model noise. As such, one challenge of PARAFAC modelling for longitudinal microbiome data is selecting the appropriate number of components. A model with the correct number of components will (1) converge quickly, (2) not have highly similar loading vectors in any mode, (3) describe meaningful biological phenomena and (4) describe these phenomena even when one or more samples are removed from the data.

Various diagnostics and methods have been proposed and need to be manually examined to determine the appropriate number of components for a PARAFAC model [36]. We propose a two-step approach for selecting the correct number of components. First, we investigate quick convergence and similarity of the loading vectors by randomly initializing a number of PARAFAC models for 1-5 components. Next, we investigate the stability of the model using a jack-knife procedure while keeping the initialized vectors the same using a singular value decomposition. In the supplied R package, this procedure is automatically performed and visualized for inspection by

305 the user with the functions assessModelQuality() and assessModelStability(), respectively. All
306 output plots examined to select the number of components for each dataset are shown in
307 **Supplementary Figures**.

308 *Metrics for assessing the appropriate number of components*

309 For each dataset, we have investigated PARAFAC models with 1-5 components and a number of
310 random initializations, depending on the size of the data and how quickly the models converge. In
311 the supplied R package, this procedure is automatically performed and visualized for inspection by
312 the user with the function assessModelQuality(). We examine the following metrics of interest.

313 In PCA, the residual sum-of-squares are plotted against the number of components in a scree-plot
314 [37, 38]. The appropriate number of components is then the area of the plot where the residual sum-
315 of-squares flattens out. For PARAFAC this principle holds as well [18].

316 The alternating least-squares implementation of PARAFAC that is used throughout this paper
317 iteratively updates the loading vectors until the convergence threshold is reached. Therefore, the
318 number of iterations needed to converge is a useful metric to inspect for the correct number of
319 components. Randomly initialized PARAFAC models with the correct number of components
320 should converge quickly compared to models with an extra component modelling noise.

321 The core consistency diagnostic (CORCONDIA) indicates how well the assumed tri-linearity of the
322 PARAFAC model holds [39]. The range of CORCONDIA is typically 0-100 but can be negative. The
323 number of components in PARAFAC models with a CORCONDIA of 50-100 can be considered
324 appropriate [18, 39].

325 The components of a PARAFAC model are non-orthogonal by default, which can sometimes lead
326 to very similar loading vectors if the model cannot be estimated properly. The Tucker congruence
327 coefficient identifies this similarity between pairs of loading vectors of the same mode [40, 41]. A
328 value in the range of 0.85-0.94 suggests that the loading vectors are fairly similar, whereas a value
329 of 0.95-1 means that the loading vectors are essentially equal [40]. The Tucker congruence
330 coefficient in the `parafac4microbiome` package uses the implementation from the multiway R
331 package (version 1.0-6; [19]).

332 *Assessing model stability through the jack-knifing of samples*

333 We expect a PARAFAC model with the correct number of components to describe meaningful
334 biological phenomena, even when one or several samples are removed from the data. We test this
335 by performing iterative jack-knifing of samples [42]. In the supplied R package, this procedure is
336 automatically performed and visualized for inspection by the user with the function
337 assessModelStability(). With this jack-knifing approach, one random sample is removed in every
338 iteration, after which a PARAFAC model is fitted to the data. We perform balanced jack-knifing,
339 removing one sample from every subject group in every iteration, if such subject metadata is
340 available. If this is impossible due to unequally sized groups, samples are randomly chosen. We
341 choose to initialise the modelling algorithm using a singular value decomposition for every iteration
342 to ensure that instability can only be caused by the removed sample(s). A PARAFAC model with
343 the correct number of components will be stable (i.e. have a small standard deviation for every
344 loading) across all jack-knifing iterations.

345 *Post-hoc clustering of PARAFAC loadings*

346 Clustering of the feature loadings can help identify groups of microbiota that are connected to a
347 particular time profile in the PARAFAC model. We performed the clustering procedure of the
348 feature loadings as follows. In accordance with the original analysis in van der Ploeg et al. [8],
349 features were not considered if the variation explained by the model for their entire time trajectory
350 was lower than the average or the congruence loading of the feature was lower than 0.4 [43]. The
351 remaining features were then clustered based on their modelled time trajectories using the K-
352 medoids algorithm from the cluster R package (v2.1.4; [44]) with 50 random starts to be robust
353 against outliers. The number of clusters was determined using the within-cluster sum of squares,
354 silhouette width and gap statistic metrics as reported by the factoextra R package (**Supplementary**
355 **Figure 17**; v1.0.7; [45]).

356 **Results**

357 *PARAFAC can identify the main time-resolved variation in longitudinal microbiome data*

358 The first example is a long time series of experimental in vitro microbiomes [6]. We analyse only
359 one experimental set-up, the aquatic microbiome culture in a peptone medium, which was
360 performed in eight replicates and measured daily for 110 days. With this example, we aim to
361 visualize the main time-resolved variation that can be modelled through PARAFAC.

362 We inspected the unprocessed count data by computing the relative abundances for every replicate
363 culture at every time point (**Figure 3A**). In most samples, 2 amplicon sequence variants (ASVs)
364 belonging to *Aeromonas* spp. comprised most of the counts. The exceptions were: the emergence of
365 *Cedecea*, *Burkholderia-Caballeronia-Paraburkholderia*, and *Pandoraea* species between days 50-110
366 in replicate culture 4, the emergence of *Clostridioides mangenotii* and a *Lachnoclostridium* species
367 between days 80-100 in replicate cultures 4 and 8, the disappearance of a *Salmonella*, *Propionivibrio*,
368 *Microbacter* and *Herbaspirillum* species between days 0-60 in replicate culture 3, the transient
369 appearance of a *Microbacter* species in replicate cultures 2 and 8, and a (small) increase in a
370 *Salmonella* species between days 100-110 in most replicate cultures. There was no clear time profile
371 visible that all replicates had in common.

372 We inspected PARAFAC modelling performance and stability for the processed count data using 1-
373 5 components. The core consistency diagnostic (CORCONDIA) scores dropped below 80 for 5
374 components. The three and four-component models explained 38.78% and 45.08% on average,
375 respectively (**Supplementary Figure 2**). Performing a jack-knifing procedure showed that the three-
376 component PARAFAC models were more stable than the four-component models (**Supplementary**
377 **Figures 3-4**). Hence, we selected the model explaining the most variation from all randomly
378 initialized models of three components. The selected model explained 39.0% of the variation (**Figure**
379 **3B**).

380 As expected, the selected PARAFAC model did not describe *Aeromonas* ASVs, because these do not
381 vary strongly over time. The first component described the disappearance of a *Salmonella*,
382 *Propionivibrio*, *Microbacter* and *Herbaspirillum* species between days 0-60, which is unique to
383 replicate 3. The second component described the emergence of a *Cedecea*, *Burkholderia-*
384 *Caballeronia-Paraburkholderia* and *Pandoraea* species between days 50-110, which is unique to
385 replicate 4. The third component described the emergence of *Clostridioides mangenotii* and a
386 *Lachnoclostridium* species between days 80-100 in replicates 4 and 8. Some of these microbiota may
387 have low relative abundances, but can still describe meaningful differences between the replicates.

388 While this example highlights the strength of PARAFAC: identifying and modelling the largest
389 sources of variation in a longitudinal microbiome dataset, the PARAFAC model only described the
390 variation partially (39%). As a result, the transient appearance of a *Herbaspirillum* species in
391 replicate cultures 2, 3 and 8, nor the (small) increase in a *Salmonella* species between days 100-110
392 in most replicate cultures, were not modelled.

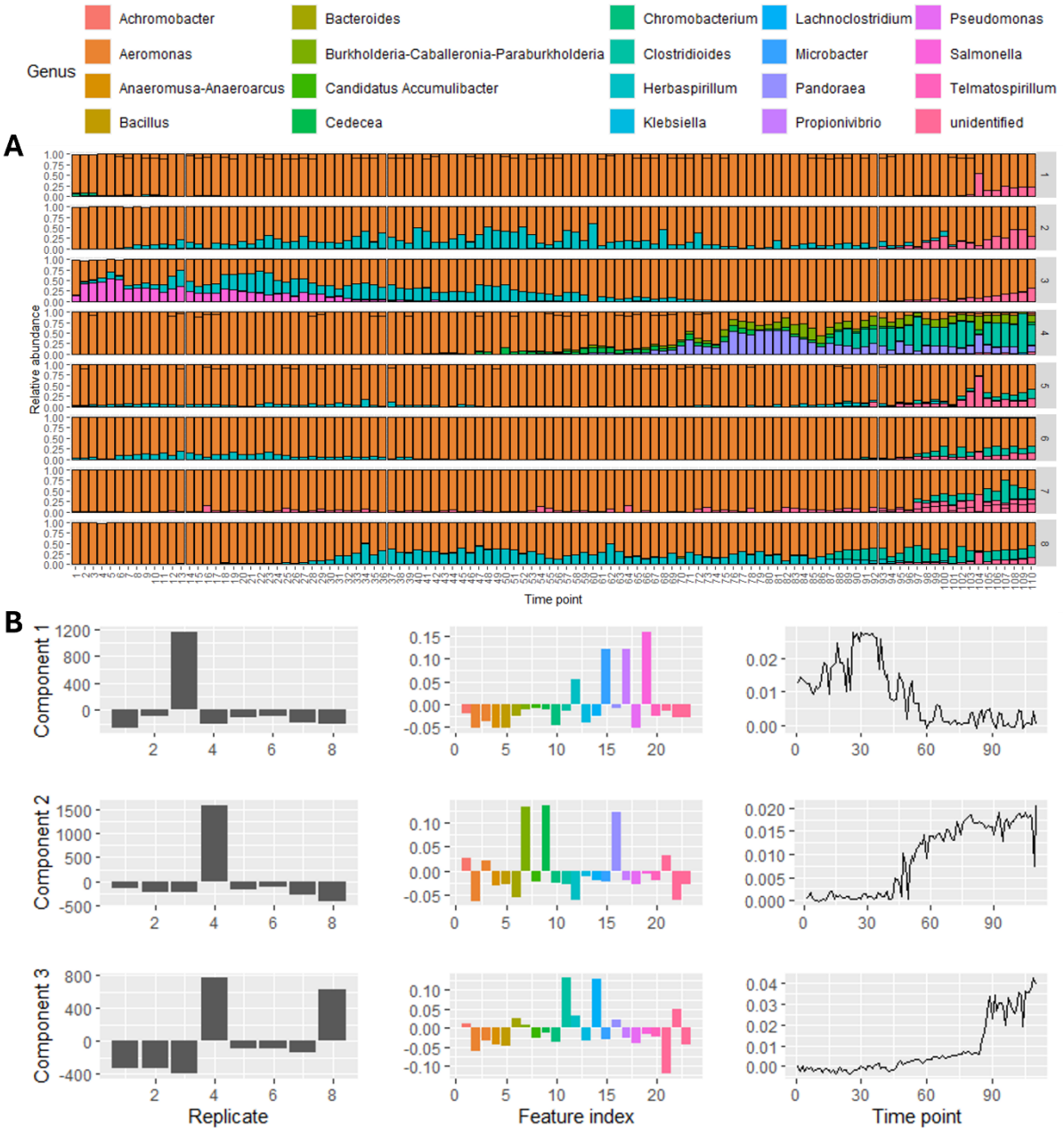

Figure 3: Overview of the Fujita et al., 2023 dataset. (A) Relative abundance plot of the dataset, split per replicate. In most samples, Aeromonas species comprise the vast majority of the counts. In the latter half of the samples in replicate 4 and the first half of the samples in replicate 3 other species are present that comprise the majority. There is no clear time profile visible that all replicates have in common. (B) The best three-component PARAFAC model of the processed data describing 39.0% of the variation. The components are shown in the rows, while the replicate, microbial abundance and time modes are shown in the columns. The first component describes the disappearance of a Salmonella, Propionivibrio, Microbacter and Herbaspirillum species between days 0-60, which is unique to replicate 3. The second component describes the emergence of a Cedecea, Burkholderia-Caballeronia-Paraburkholderia and Pandoraea species between days 50-110, which is unique to replicate 4. The third component describes the emergence of Clostridioides mangenotii and a Lachnoclostridium species between days 80-100 in replicates 4 and 8.

405 *PARAFAC finds differences between subject groups and enhances comparative analyses*

406 The second example is a longitudinal infant faecal microbiome study [7]. Samples were collected
407 from 314 vaginally born and 282 caesarean-section born infants at four time points: 4, 7 and 21 days
408 after birth and a follow-up sample during infancy (between 4-12 months after birth). One of the
409 four measurements is missing for most infants in this cohort, and we keep the missing data in the
410 data cube for the PARAFAC algorithm to impute (**Supplementary Table 1-2**). With this example,
411 we show how PARAFAC can identify the differences between the subject groups and enhance the
412 comparative analysis done by the original authors despite a moderate amount of missing data.

413 The authors stated that there was a very clear distinction in the microbiomes of vaginally and
414 caesarean-section born children, also over time. To analyse this distinction, we inspected the
415 unprocessed count data by computing the average relative abundance for the vaginal and caesarean
416 groups at every time point (**Figure 4A**). This confirmed a clear difference at the phylum level
417 between the vaginal and caesarean groups at day 4, 7 and 21, which disappeared in infancy.

418 We inspected PARAFAC modelling performance and stability for the processed count data using 1-
419 5 components. The CORCONDIA scores dropped below 80 at 3-5 components (**Supplementary**
420 **Figure 6**). Performing a jack-knifing procedure showed that the two-component model as stable as
421 the three-component model (**Supplementary figures 7-8**). Hence, we selected the model explaining
422 the most variation from all randomly initialized models of three components. The selected model
423 explained 9.40% of the variation (**Figure 4B**).

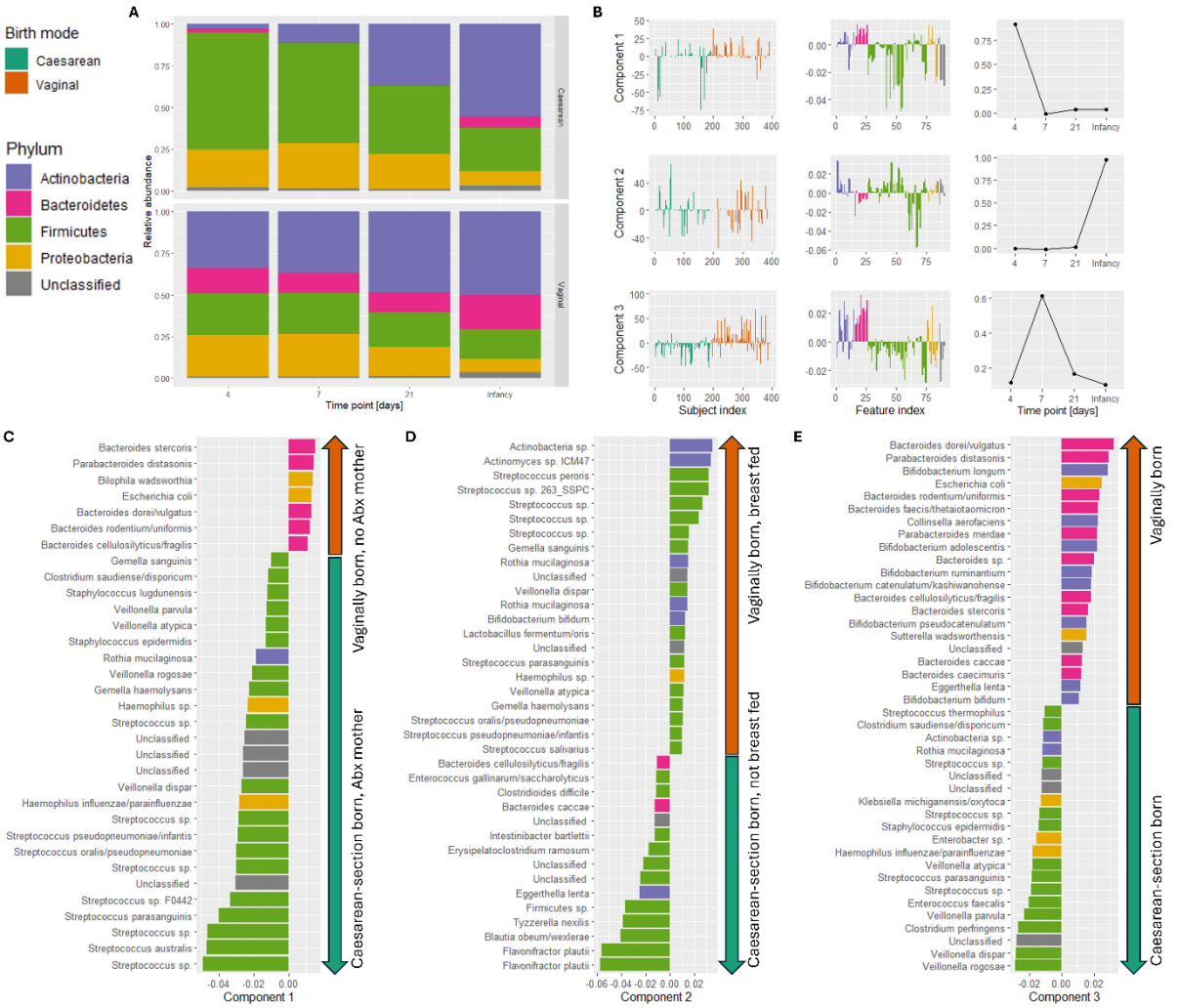

Figure 4: Overview of the Shao et al., 2019 dataset. (A) Overview of the average relative abundance per time point in vaginal and caesarean-section born infants. The birth mode groups are distinguishable between time points 4 and 21 and become similar at infancy. (B) The best three-component PARAFAC model of the processed data, explaining 9.40% of the variation. Components 1-3 all describe differences between the birth mode groups. Component 1, mainly present on day 4, additionally describes differences based on antibiotics being given to the mother during labour. Component 2, mainly present during infancy, additionally describes feeding mode. Component 3 describes only describes differences between the birth mode groups, which are present throughout the study but are largest on day 7. (C) Loadings of the microbiota in component 1. Positively loaded microbiota are associated with vaginally born infants and/or mothers having received antibiotics during labour. Negatively loaded microbiota are associated with caesarean-section born infants and/or mothers not having received antibiotics during labour. (D) Loadings of the microbiota in component 2. Positively loaded microbiota are associated with vaginally born and/or breast-fed infants. Negatively loaded microbiota are associated with caesarean-section born and/or not breast-fed infants. (E) Loadings of the microbiota in component 3. Positively loaded microbiota are associated with vaginally born infants. Negatively loaded microbiota are associated with caesarean-section born infants. Feature loadings in (C-E) are filtered to only show loadings with an absolute value higher than 0.01. For the unfiltered version of these plots, see Supplementary Figures 9-11.

All components of the selected model described differences in birth mode (p=2.4e-4, p=7.3e-9 and p=1.2e-46, respectively; Benjamini-Hochberg corrected Wilcoxon rank-sum test; **Supplementary Table 3**) and differences based on the *Bacteroides* profile as described by the original authors based on the median relative abundance of the genus (p=1.5e-4, p=7.3e-9, p=8.7e-59, respectively; [7]). In addition, the first component described differences related to whether antibiotics were given to the

445 mother during labour (p=0.0059) and the second component described differences based on feeding
446 method (p=0.024).

447 Inspection of the positive loadings in the first component revealed that PARAFAC described the
448 genera that were enriched in vaginally born infants: *Bacteroides stercoris, Parabacteroides*
449 *distasonis, Bilophilia wadsworthia, Escherichia coli, Bacteroides dorei/vulgatus, Bacteroides*
450 *rodentium/uniformis and Bacteroides cellulosilyticus/fragilis* (**Figure 4C**). These genera were
451 depleted in caesarean-section born infants and infants whose mothers received antibiotics during
452 labour. The first component also described genera that were enriched in caesarean-section born
453 infants or infants whose mothers received antibiotics during labour: *Streptococcus australis,*
454 *Streptococcus parasanguinis, Streptococcus oralis,* amongst others. These genera were depleted in
455 vaginally born infants.

456 Inspection of the positive loadings in the second component revealed that PARAFAC described the
457 genera that were enriched in vaginally born or breast-fed infants: *Actinobacteria sp., Actinomyces*
458 *sp. ICM47,* and *Streptococcus peroris,* amongst others (**Figure 4D**). These genera were depleted in
459 caesarean-section born and formula-fed infants. It also described the genera that were enriched in
460 caesarean-section born or formula-fed infants: *Flavonifractor plautii, Blautia obeum/wexlerae* and
461 *Tyzzerella nexilis,* amongst others. These genera were depleted in vaginally born and breast-fed
462 infants. While not described in the original analysis, these results partially agree with other
463 literature [46–48].

464 Inspection of the positive loadings in the third component revealed that PARAFAC described the
465 genera that were enriched in vaginally born infants: *Bacteroides dorei/vulgatus, Parabacteroides*
466 *distasonis* and *Bifidobacterium longum,* amongst others (**Figure 4E**). These genera were depleted in
467 caesarean-section born infants. It also described the genera that were enriched in caesarean-section
468 born infants: *Veillonella rogosae, Veillonella dispar,* and *Clostridium perfringens,* amongst others.
469 These genera were depleted in vaginally born infants. This result is consistent with the original
470 analysis and other studies investigating the development of the infant gut microbiome in hospital
471 environments [46, 47].

472 Taken together, the PARAFAC model of this example dataset confirmed previously found
473 differences between the caesarean-section and vaginally born infants. It also found novel genera
474 that describe the differences between the birth mode groups and feeding mode groups. Additionally,

475 the moderate (62.5%) amount of missing data did not hamper the modelling procedure. In summary,
476 the PARAFAC model of this dataset confirms and enhances the results from the comparative
477 analysis done by the original authors.

478 *Post-hoc clustering of PARAFAC results can help identify microbial groups of interest*

479 The third example is a longitudinal oral microbiome gingivitis intervention study [8]. Here, we
480 analyse one oral microbiome niche, the supragingival plaque at the upper jaw lingual surfaces,
481 which was measured in 41 subjects at 7 time points: day -14 (baseline), 0 (baseline, start of
482 intervention), 2, 5, 9, 14 (end of intervention) and 21 (resolution). Using quantitative light-induced
483 fluorescence [33–35], the subjects were stratified into low, medium and high responders based on
484 the amount of red fluorescent dental plaque on day 14. With this example, we show how a post-hoc
485 clustering approach of a PARAFAC model can help identify groups of microbiota related to the
486 intervention.

487 We inspected PARAFAC modelling performance and stability for the processed count data using 1-
488 5 components. The CORCONDIA scores dropped below 80 for 5 components and the sum of squared
489 errors began to flatten between 2-3 components (**Supplementary Figure 13**). The three-component
490 models had very similar feature and time mode loadings between several components, making them
491 not suitable for describing the data (**Supplementary Figure 14**). This was confirmed by the jack-
492 knifing procedure (**Supplementary Figures 15-16**). Hence, we selected the model explaining the
493 most variation from all randomly initialized models of two components. The selected model
494 explained 19.21% of the variation (**Figure 5A**).

495

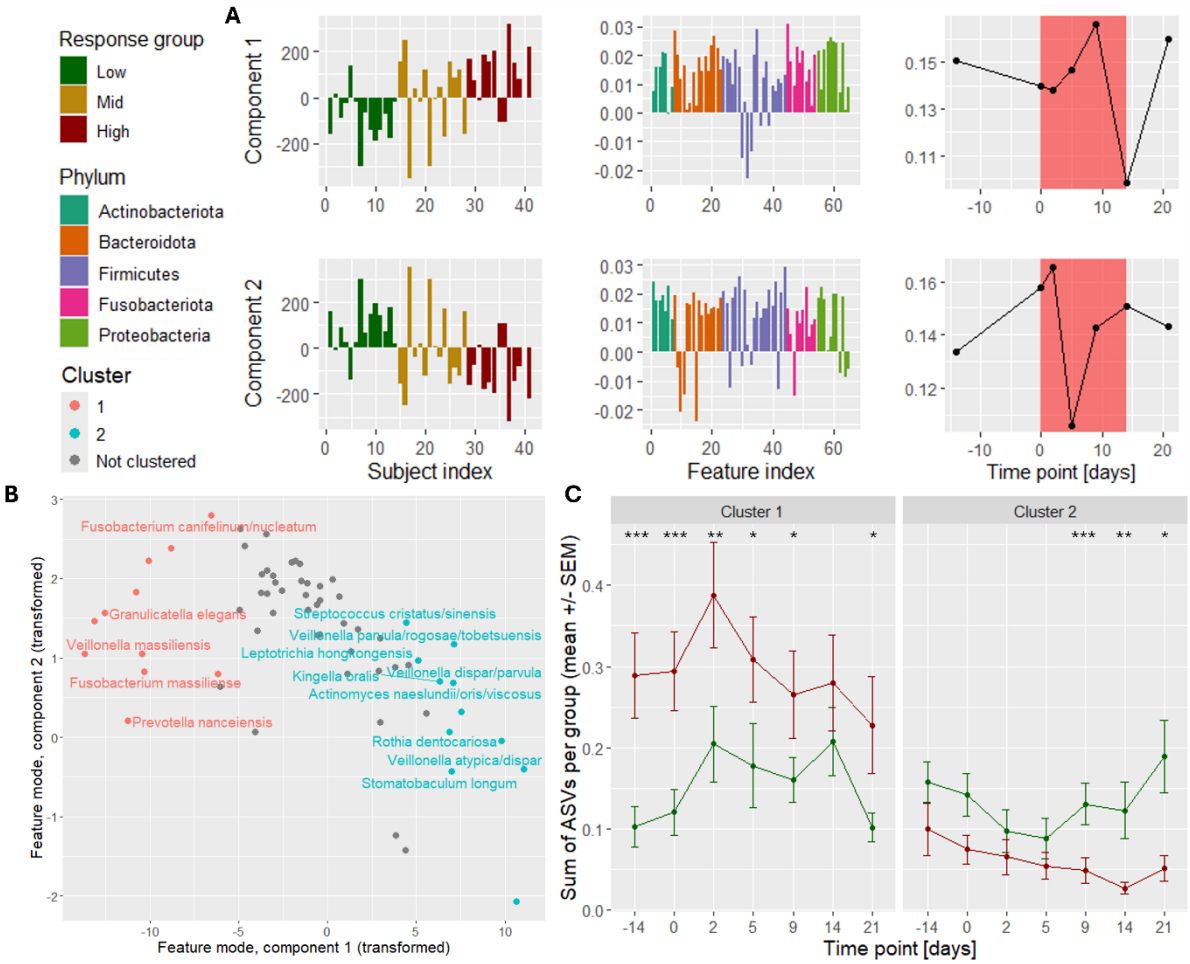

Figure 5: Overview of the van der Ploeg et al., 2024 dataset. (A) The best two-component PARAFAC model of the processed data, explaining 19.21% of the variation. Both components describe differences between the response groups that are relatively constant throughout the study. The time profile in component 1 describes that the differences between the response groups are larger on day 2 and much smaller on day 5. The time profile in component 2 describes that the differences between the response groups are larger on day 9 and much smaller on day 14. (B) Scatter plot showing the transformed feature loadings (Supplementary Methods) of PARAFAC component 1 versus component 2. Features were clustered into two groups after filtering. Only amplicon sequence variants (ASVs) with taxonomic annotations resolved to species level are labelled. (C) Overview of the relative abundance sum per ASV cluster in the low and high response groups. Error bars correspond to the standard error of the mean (SEM) across all samples per response group. The mean difference between the high and low response groups per time point was tested using a Benjamini-Hochberg corrected permutation test of 999 iterations (: p≤0.05; **: p≤0.01; ***: p≤0.001). Mid responders are not shown for visual clarity.*

To interpret the models, we tested the correlation of the subject loadings with the measured parameters of gingivitis. This approach revealed that both components of the PARAFAC model significantly described the amount of red fluorescent plaque over time (p=1.6e-5 and p=0.037, respectively; Benjamini-Hochberg corrected Pearson correlation test; **Supplementary Table 4**) and the percentage of sites that were covered by plaque (p=0.030 and p=0.037, respectively).

Following the original analysis [8], we identified microbial subcommunities with common responses by selecting and then clustering well-modelled amplicon sequence variants (ASVs) based on their fitted response (**Figure 5B**). The sum of the relative abundances of the ASVs in each cluster

was then determined to test the difference between the microbiomes of individuals in the low and high response groups at every time point. This approach revealed that the relative abundance sum of ASV cluster 1 was significantly higher in the high responder individuals compared to the low responder individuals on days -14, 0, 2, 5, 9 and 21 (**Figure 5C, Supplementary Table 5**; $p \leq 0.05$; Benjamini-Hochberg corrected permutation test of mean difference). Similarly, the relative abundance sum of ASV cluster 2 was found to be significantly higher in low responder individuals compared to high responder individuals on days 9, 14 and 21. Taken together, the PARAFAC models of plaque microbiomes described microbial subcommunities with common dynamics that connect to the magnitude of the gingivitis response.

Discussion

Using three example studies [6–8], we show that the unsupervised modelling approach of Parallel Factor Analysis (PARAFAC) can (1) identify the main time-resolved variation in longitudinal microbiome data, (2) find differences between subject groups and enhance comparative analyses and (3) helps identify feature groups of interest using a post-hoc clustering approach. In addition, we show that PARAFAC is robust to missing measurements in the Shao et al., 2019 [7] example. Robustness of the PARAFAC algorithm in the context of missing data was an expected result and is well-documented [48, 49]. We also show in the Shao et al., 2019 [7] and van der Ploeg et al., 2024 [8] examples that the modelled variation is related to clinically relevant parameters. However, many other multi-way approaches exist that are more flexible in their modelling procedure [30]. For example, Tucker3 allows for interactions between the components [50]. PARAFAC2 allows for time shifts that are unique per subject [18, 51]. Multi-way regression, in which the PARAFAC components are supervised using a response variable, is also possible with N-way partial least squares [52]. As highlighted in the Fujita et al. example study [6], these multi-way dimension reduction methods require commonality between the subjects to be useful. Further research is needed to investigate the relevance of these methods in the context of longitudinal microbiome data analysis.

In PARAFAC, the nature of the third mode in the multi-way array is not limited to time. For example, a recent study has shown that soil treatment can be used as the third mode to identify relationships between the abundances of mycorrhizal fungi and plant diversity and history [53]. Additionally, the principles shown in this work are generalizable to four or more modes if that better represents the data that was generated by the study design.

546 In this work we have not elaborated on the various options that exist for processing microbial
547 abundance data. The addition of a pseudo-count prior to a centred log-ratio (CLR) transformation
548 is a complex and unresolved matter [54, 55]. It has been noted that this approach introduces a
549 dependency with library size, depending on the number of zeroes in the data [54]. Other work [55]
550 suggests that a sample-specific pseudo-count may resolve this issue, but further research is needed
551 to examine this approach in the context of longitudinal microbiome data. Other options include
552 setting a pseudo-count value of 0.5, 0.1 or replacing the zeroes with a random value between 0 and
553 1 drawn from a uniform distribution. We conducted a brief sensitivity analysis for these options
554 (**Supplementary Figure S18**) and decided to use a pseudo-count of 1 as this treats all zeroes as
555 relevant values while yielding similar models. In a related paper on tensor factorization of
556 longitudinal microbiome data [56] the robust-centred log-ratio was suggested as an approach to
557 transform the data and to correct for compositionality. This approach instead calculates the
558 geometric mean by ignoring the zeroes and setting them to missing values after the transformation.
559 This makes all zeroes available for imputation by the PARAFAC model, but ignores the different
560 nature that zeroes can potentially have [26]. Further research is needed to investigate the
561 appropriateness of the various processing methods for (longitudinal) microbiome count data in
562 describing biological phenomena of interest.

563 Conclusions

564 We have shown that Parallel Factor Analysis is an applicable method for longitudinal microbiome
565 data analysis across a wide range of microbial environments. Our results demonstrate that
566 PARAFAC is able to (1) model the main time-resolved variation in longitudinal microbiome data,
567 (2) find differences between subject groups and enhance comparative analyses despite a moderate
568 amount of missing data, and (3) help identify feature groups of interest. The analyses and the
569 example datasets with the resulting figures are implemented in the R package
570 `parafac4microbiome`, which is available on CRAN at
571 https://cran.rstudio.com/web/packages/parafac4microbiome/.

572 List of abbreviations

573 - ALS: Alternating Least-Squares
574 - ASV: Amplicon Sequence Variant
575 - CLR: Centred Log-Ratio
576 - CORCONDIA: Core Consistency Diagnostic

- mOTU: Marker-gene based Operational Taxonomic Unit
- PCA: Principal Component Analysis
- PARAFAC: Parallel Factor Analysis

Ethics approval and consent to participate

Not applicable.

Consent for publication

Not applicable.

Availability of the data and materials

The package used during the current study is available in the GitHub repository, https://doi.org/10.5281/zenodo.13862690. The datasets generated and/or analysed during the current study are available in the GitHub repository, https://doi.org/10.5281/zenodo.13908878.

Competing interests

The authors declare that they have no competing interests.

Funding

GRvdP was funded by a grant from the University of Amsterdam, Research Priority Area on Personal Microbiome Health.

Authors' contributions

G.R. van der Ploeg: conceptualization, visualization, formal analysis, methodology, programming, writing – original draft; J.A. Westerhuis: conceptualization, methodology, supervision, formal analysis, writing – original draft; A. Heintz-Buschart: conceptualization, formal analysis, supervision, project administration, writing – original draft; A.K. Smilde: conceptualization, methodology, supervision, funding acquisition, writing – review & editing.

Acknowledgements

We want to thank Jesse Alderliesten (UU/UvA) for their useful discussions and suggestions.

References

1. Lloyd-Price J, Arze C, Ananthakrishnan AN, Schirmer M, Avila-Pacheco J, Poon TW, et al. Multi-omics of the gut microbial ecosystem in inflammatory bowel diseases. Nature. 2019;569:655–62.

2. Pascal M, Perez-Gordo M, Caballero T, Escribese MM, Lopez Longo MN, Luengo O, et al. Microbiome and Allergic Diseases. Front Immunol. 2018;9.

3. Saus E, Iraola-Guzmán S, Willis JR, Brunet-Vega A, Gabaldón T. Microbiome and colorectal cancer: Roles in carcinogenesis and clinical potential. Mol Aspects Med. 2019;69:93–106.

4. Gerber GK. Longitudinal Microbiome Data Analysis. In: Metagenomics for Microbiology. Elsevier; 2015. p. 97–111.

5. Schmidt TSB, Raes J, Bork P. The Human Gut Microbiome: From Association to Modulation. Cell. 2018;172:1198–215.

6. Fujita H, Ushio M, Suzuki K, Abe MS, Yamamichi M, Iwayama K, et al. Alternative stable states, nonlinear behavior, and predictability of microbiome dynamics. Microbiome. 2023;11:63.

7. Shao Y, Forster SC, Tsaliki E, Vervier K, Strang A, Simpson N, et al. Stunted microbiota and opportunistic pathogen colonization in caesarean-section birth. Nature. 2019;574:117–21.

8. van der Ploeg GR, Brandt BW, Keijser BJF, van der Veen MH, Volgenant CMC, Zaura E, et al. Multi-way modelling of oral microbial dynamics and host-microbiome interactions during induced gingivitis. Npj Biofilms Microbiomes. 2024;10:1–12.

9. Diggle P. Analysis of longitudinal data. Oxford university press; 2002.

10. Fitzmaurice GM, Laird NM, Ware JH. Applied longitudinal analysis. John Wiley & Sons; 2012.

11. Kodikara S, Ellul S, Lê Cao K-A. Statistical challenges in longitudinal microbiome data analysis. Brief Bioinform. 2022;23:bbac273.

12. Bro R, Smilde AK. Principal component analysis. Anal Methods. 2014;6:2812–31.

13. Jolliffe I. Principal Component Analysis. In: Wiley StatsRef: Statistics Reference Online. John Wiley & Sons, Ltd; 2014.

14. Carroll JD, Chang J-J. Analysis of individual differences in multidimensional scaling via an N-way generalization of “Eckart-Young” decomposition. Psychometrika. 1970;35:283–319.

15. Harshman RA. Foundations of the PARAFAC procedure: Models and conditions for an" explanatory" multimodal factor analysis. 1970.

16. Tomasi G, Bro R. A comparison of algorithms for fitting the PARAFAC model. Comput Stat Data Anal. 2006;50:1700–34.

17. Yates F. The analysis of replicated experiments when the field results are incomplete. Emp J Exp Agric. 1933;1:129–42.

18. Bro R. Multi-way analysis in the food industry. Models Algorithms Appl Acad Proefschr Dinam. 1998.

19. Helwig NE, Helwig MNE. Package ‘multiway.’ 2019.

20. Kruskal JB. More factors than subjects, tests and treatments: An indeterminacy theorem for canonical decomposition and individual differences scaling. Psychometrika. 1976;41:281–93.

21. Kruskal JB. Three-way arrays: rank and uniqueness of trilinear decompositions, with application to arithmetic complexity and statistics. Linear Algebra Its Appl. 1977;18:95–138.

22. ten Berge JMF, Sidiropoulos ND. On uniqueness in candecomp/parafac. Psychometrika. 2002;67:399–409.

23. Kruskal JB. Rank, decomposition, and uniqueness for 3-way and N-way arrays. In: Multiway data analysis. 1989. p. 7–18.

24. Aitchison J. The Statistical Analysis of Compositional Data. J R Stat Soc Ser B Methodol. 1982;44:139–60.

25. Gloor GB, Macklaim JM, Pawlowsky-Glahn V, Egozcue JJ. Microbiome Datasets Are Compositional: And This Is Not Optional. Front Microbiol. 2017;8:2224.

26. Silverman JD, Roche K, Mukherjee S, David LA. Naught all zeros in sequence count data are the same. Comput Struct Biotechnol J. 2020;18:2789–98.

27. Paulson JN, Stine OC, Bravo HC, Pop M. Differential abundance analysis for microbial marker-gene surveys. Nat Methods. 2013;10:1200–2.

28. Segata N, Izard J, Waldron L, Gevers D, Miropolsky L, Garrett WS, et al. Metagenomic biomarker discovery and explanation. Genome Biol. 2011;12:R60.

29. Bro R, Smilde AK. Centering and scaling in component analysis. J Chemom. 2003;17:16–33.

30. Smilde AK, Bro R, Geladi P. Multi-way analysis: applications in the chemical sciences. John Wiley & Sons; 2005.

31. R Core Team R. R: A language and environment for statistical computing. 2013.

32. Milanese A, Mende DR, Paoli L, Salazar G, Ruscheweyh H-J, Cuenca M, et al. Microbial abundance, activity and population genomic profiling with mOTUs2. Nat Commun. 2019;10:1014.

33. Heinrich-Weltzien R, Kühnisch J, Van Der Veen M, De Josselin De Jong E, Stößer L. Quantitative light-induced fluorescence (QLF) - A potential method for the dental practitioner. Quintessence Int. 2003;34:181–8.

34. van der Veen MH, Volgenant CMC, Keijser B, ten Cate J (Bob) M, Crielaard W. Dynamics of red fluorescent dental plaque during experimental gingivitis—A cohort study. J Dent. 2016;48:71–6.

35. Volgenant CMC, Zaura E, Brandt BW, Buijs MJ, Tellez M, Malik G, et al. Red fluorescence of dental plaque in children —A cross-sectional study. J Dent. 2017;58:40–7.

36. Bro R. PARAFAC. Tutorial and applications. Chemom Intell Lab Syst. 1997;:23.

37. Cattell RB. The Scree Test For The Number Of Factors. Multivar Behav Res. 1966;1:245–76.

38. Horn JL, Engstrom R. Cattell's Scree Test In Relation To Bartlett's Chi-Square Test And Other Observations On The Number Of Factors Problem. Multivar Behav Res. 1979;14:283–300.

39. Bro R, Kiers H. A new Efficient Method for Determining the Number of Components in PARAFAC Models. J Chemom. 2003;17:274–86.

674 40. Lorenzo-Seva U, ten Berge JMF. Tucker's congruence coefficient as a meaningful index of factor
675 similarity. Methodol Eur J Res Methods Behav Soc Sci. 2006;2:57–64.

676 41. Tucker LR. A method for synthesis of factor analysis studies. Educational Testing Service Princeton,
677 NJ; 1951.

678 42. Riu J, Bro R. Jack-knife technique for outlier detection and estimation of standard errors in PARAFAC
679 models. Chemom Intell Lab Syst. 2003;65:35–49.

680 43. Lorho G, Westad F, Bro R. Generalized correlation loadings: Extending correlation loadings to
681 congruence and to multi-way models. Chemom Intell Lab Syst. 2006;84:119–25.

682 44. Maechler M. Finding groups in data: Cluster analysis extended Rousseeuw et al. R Package Version.
683 2019;2:242–8.

684 45. Kassambara A, Mundt F. Package 'factoextra.' Extr Vis Results Multivar Data Anal. 2017;76.

685 46. Raveh-Sadka T, Firek B, Sharon I, Baker R, Brown CT, Thomas BC, et al. Evidence for persistent and
686 shared bacterial strains against a background of largely unique gut colonization in hospitalized
687 premature infants. ISME J. 2016;10:2817–30.

688 47. Stewart CJ, Skeath T, Nelson A, Fernstad SJ, Marrs EC, Perry JD, et al. Preterm gut microbiota and
689 metabolome following discharge from intensive care. Sci Rep. 2015;5:17141.

690 48. Tomasi G, Bro R. PARAFAC and missing values. Chemom Intell Lab Syst. 2005;75:163–80.

691 49. Acar E, Dunlavy DM, Kolda TG, Mørup M. Scalable tensor factorizations for incomplete data.
692 Chemom Intell Lab Syst. 2011;106:41–56.

693 50. Kroonenberg PM, De Leeuw J. Principal component analysis of three-mode data by means of
694 alternating least squares algorithms. Psychometrika. 1980;45:69–97.

695 51. Kiers HAL, Ten Berge JMF, Bro R. PARAFAC2—Part I. A direct fitting algorithm for the PARAFAC2
696 model. J Chemom. 1999;13:275–94.

697 52. Bro R. Multiway calibration. Multilinear PLS. J Chemom. 1996;10:47–61.

698 53. Albracht C, Solbach MD, Hennecke J, Bassi L, Van Der Ploeg GR, Eisenhauer N, et al. Common soil
699 history is more important than plant history for arbuscular mycorrhizal community assembly in an
700 experimental grassland diversity gradient. preprint. Microbiology; 2024.

701 54. Te Beest DE, Nijhuis EH, Möhlmann TWR, Ter Braak CJF. Log-ratio analysis of microbiome data with
702 many zeroes is library size dependent. Mol Ecol Resour. 2021;21:1866–74.

703 55. Erhard F. Estimating pseudocounts and fold changes for digital expression measurements.
704 Bioinformatics. 2018;34:4054–63.

705 56. Martino C, Morton JT, Marotz CA, Thompson LR, Tripathi A, Knight R, et al. A Novel Sparse
706 Compositional Technique Reveals Microbial Perturbations. mSystems. 2019;4:e00016-19.

707

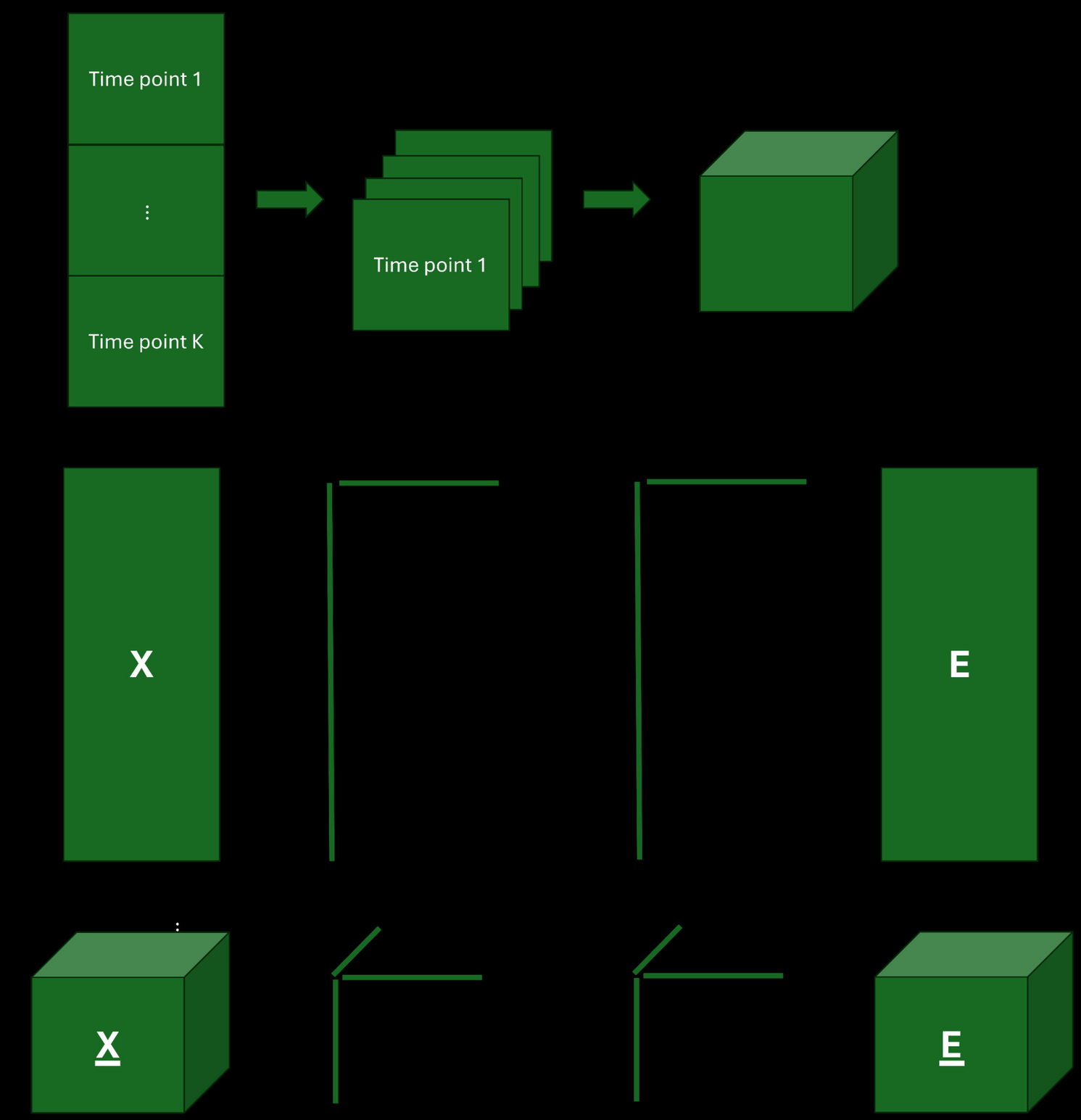
Time point 1
⋮
Time point K
Time point 1
X
E
X
E

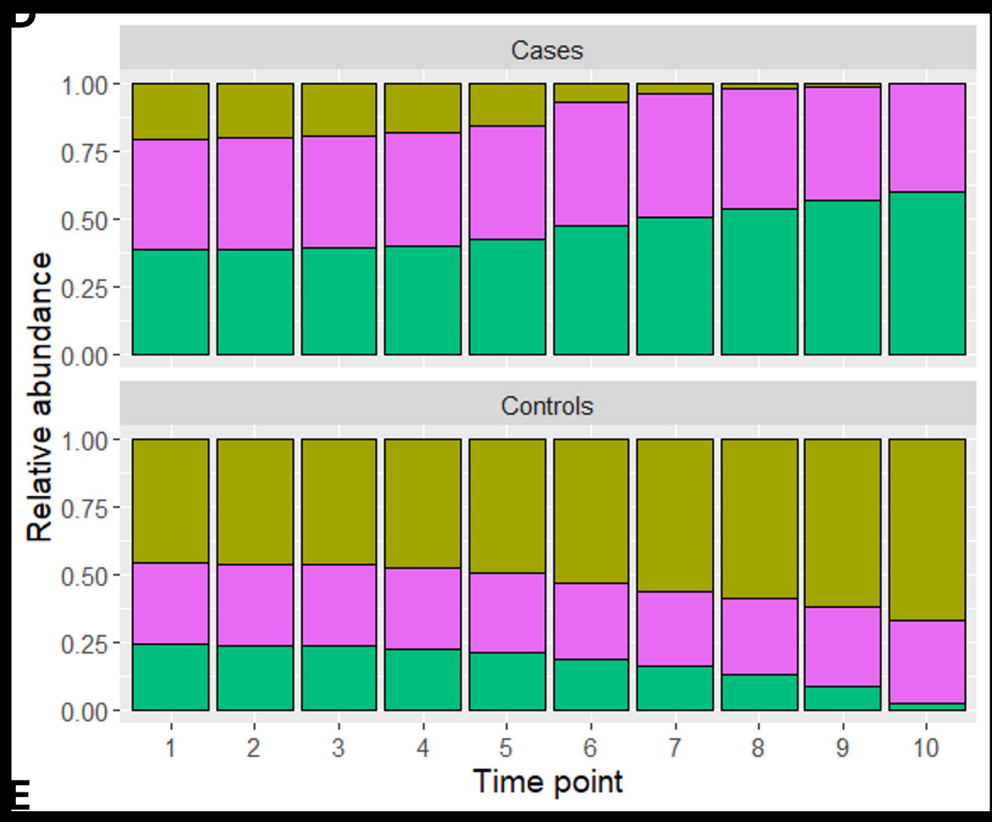
Cases
Controls
Relative abundance
1.00
0.75
0.50
0.25
0.00
1 2 3 4 5 6 7 8 9 10
Time point

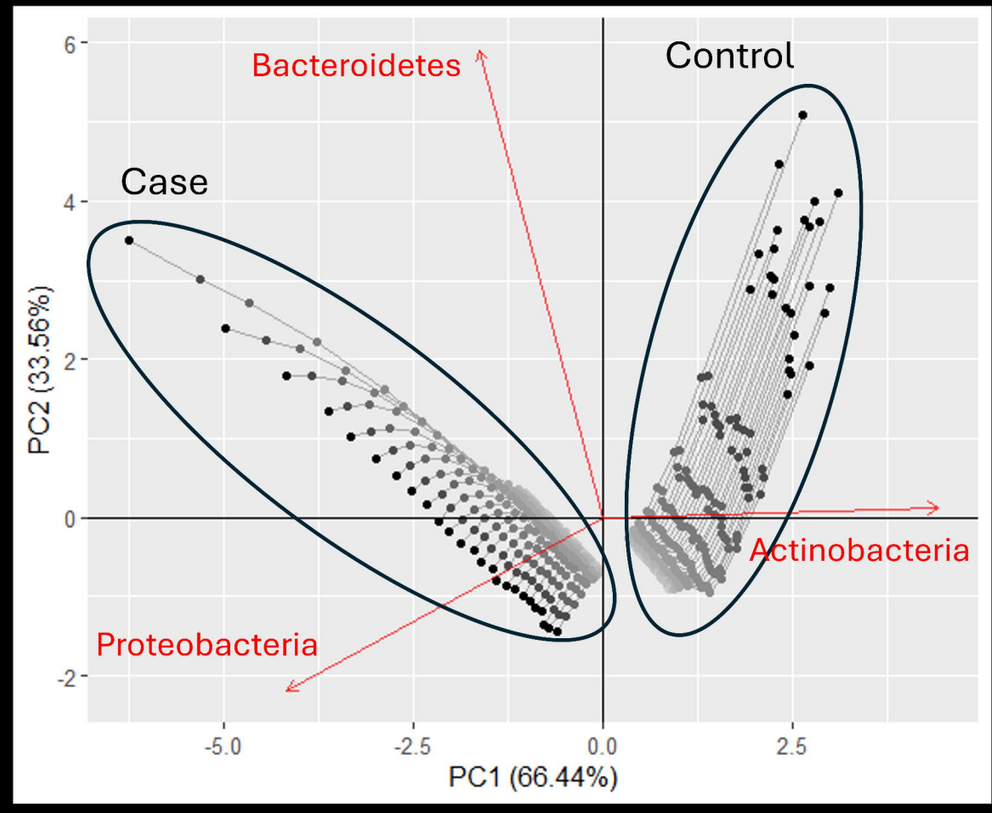
Bacteroidetes
Control
Case
Actinobacteria
Proteobacteria
PC2 (33.56%)
PC1 (66.44%)
6
4
2
0
-2
-5.0
-2.5
0.0
2.5

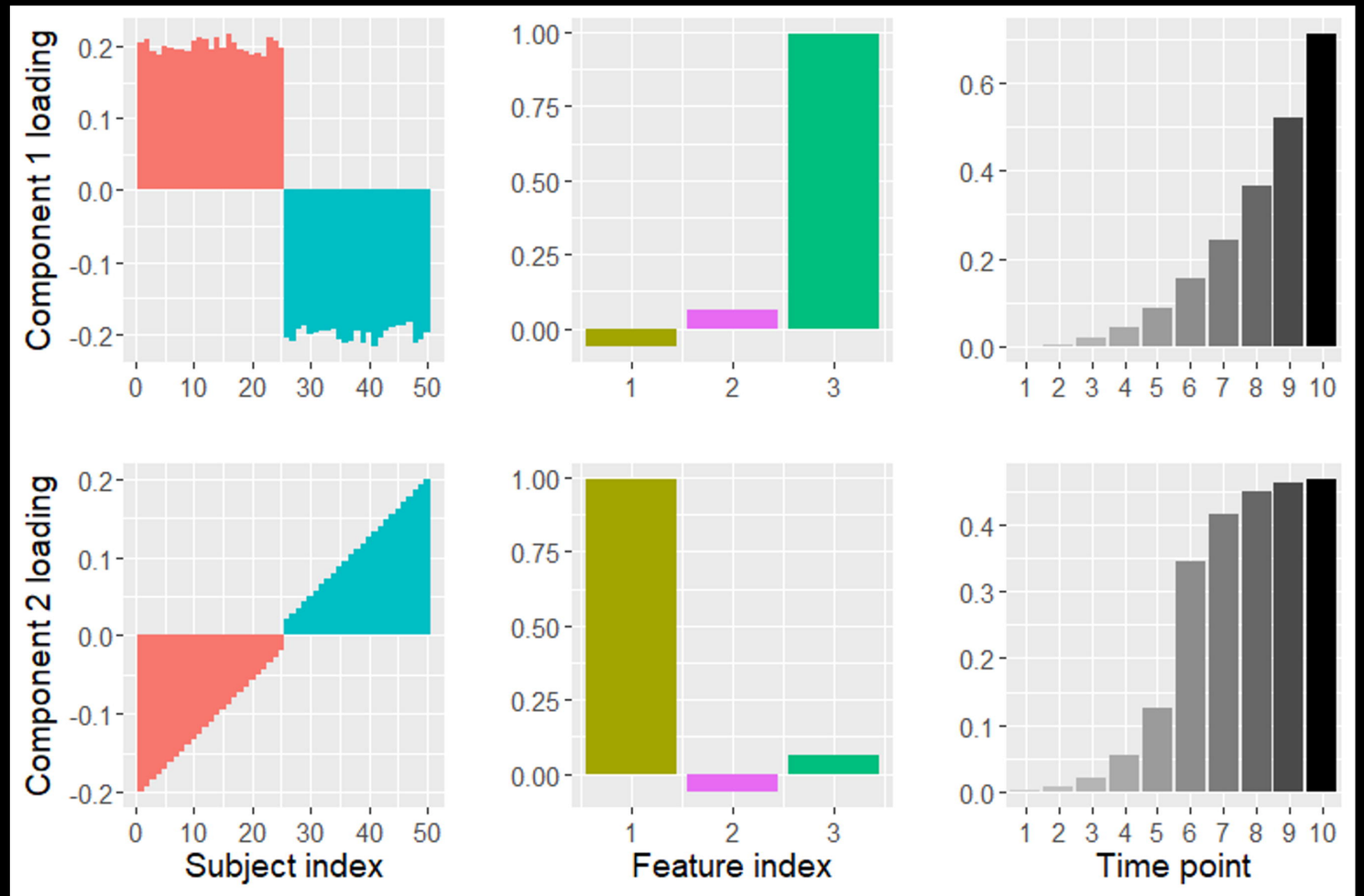
Component 1 loading
Component 2 loading
Subject index
Feature index
Time point

Subject group
Case
Control

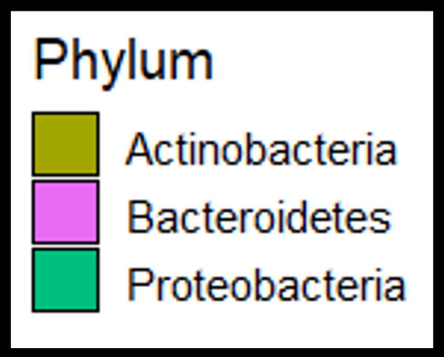
Phylum
Actinobacteria
Bacteroidetes
Proteobacteria

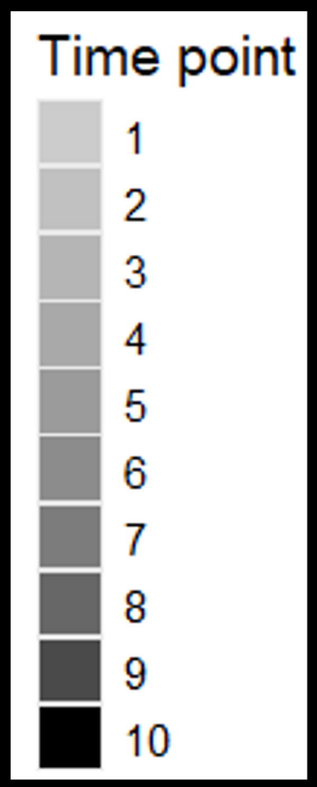
Time point
1
2
3
4
5
6
7
8
9
10

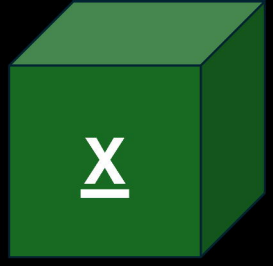

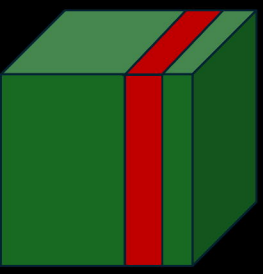

Filtering based on sparsity across all measurements

Centred log-ratio transformation per measurement

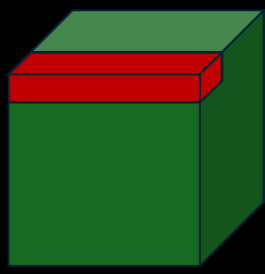

Centring across the subject mode

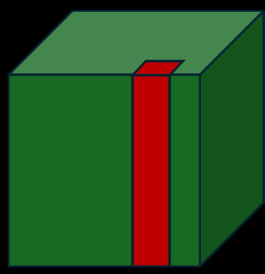

Scaling within the feature mode

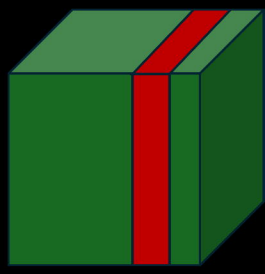

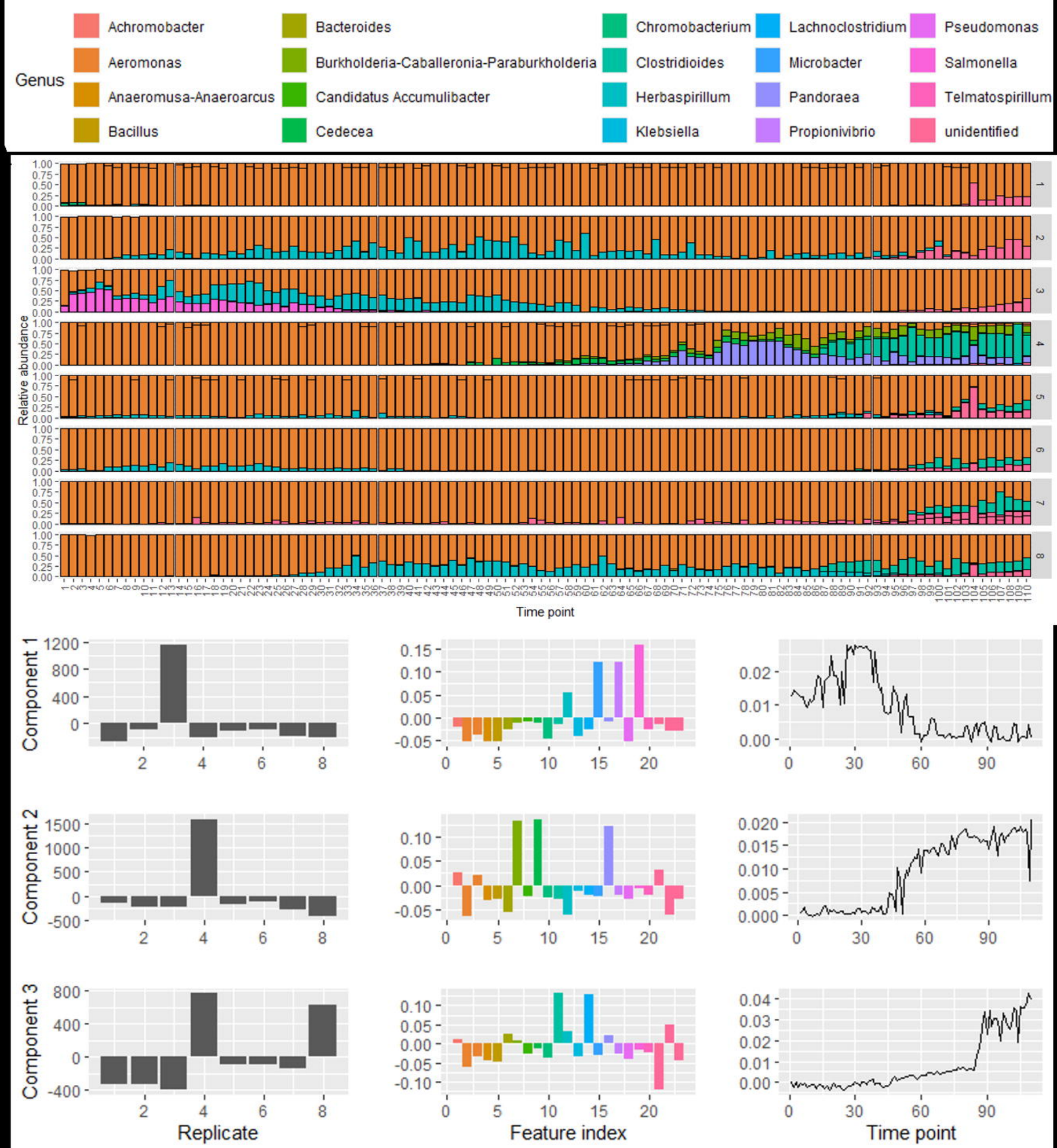
Genus
Achromobacter
Aeromonas
Anaeromusa-Anaeroarcus
Bacillus
Bacteroides
Burkholderia-Caballeronia-Paraburkholderia
Candidatus Accumulibacter
Cedecea
Chromobacterium
Clostridioides
Herbaspirillum
Klebsiella
Lachnoclostridium
Microbacter
Pandoraea
Propionivibrio
Pseudomonas
Salmonella
Telmatospirillum
unidentified
Relative abundance
Time point
Component 1
Component 2
Component 3
Replicate
Feature index
Time point

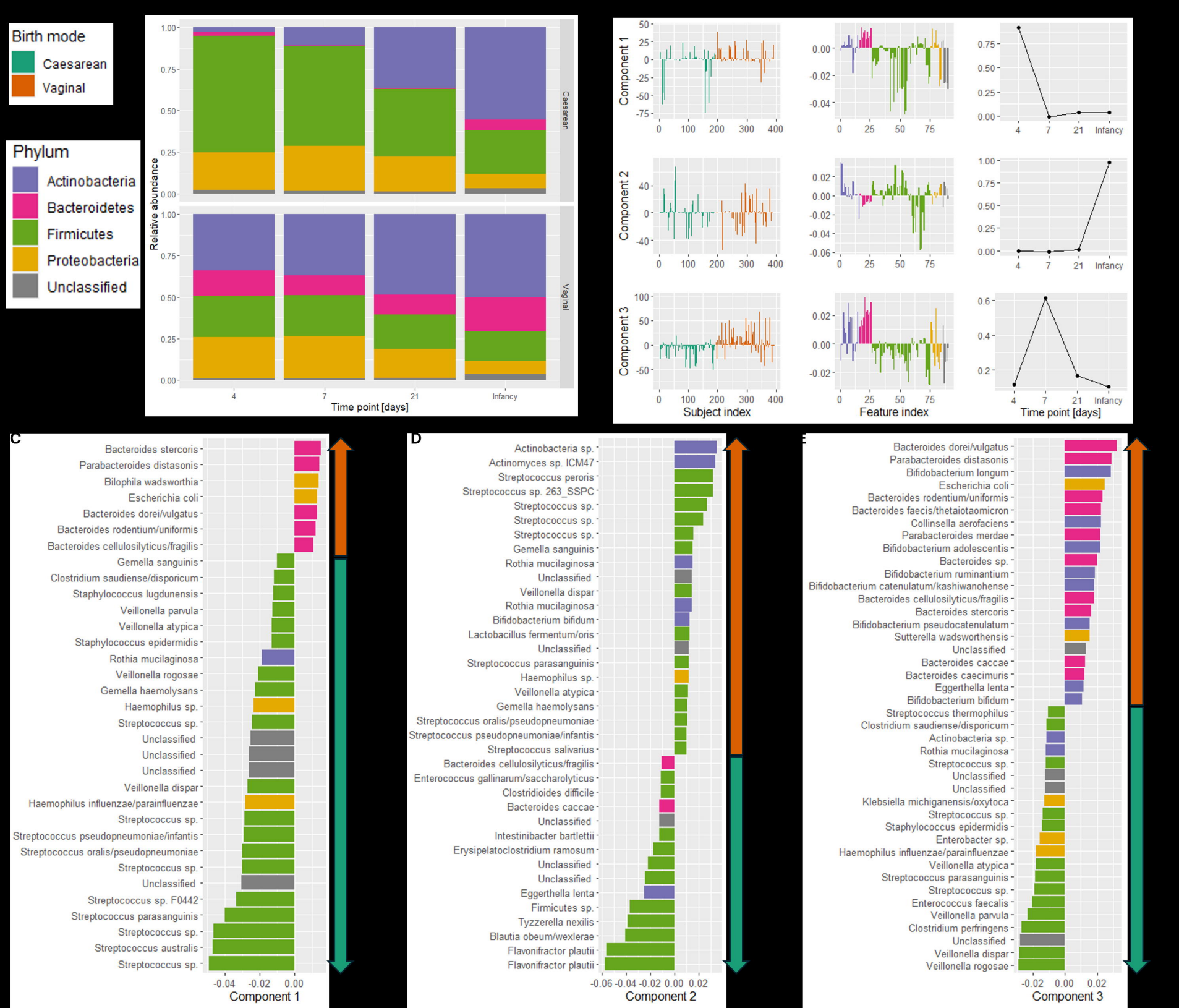
Birth mode
Caesarean
Vaginal
Phylum
Actinobacteria
Bacteroidetes
Firmicutes
Proteobacteria
Unclassified
Relative abundance
Caesarean
Vaginal
Time point [days]
Infancy
Component 1
Component 2
Component 3
Subject index
Feature index
C
Bacteroides stercoris
Parabacteroides distasonis
Bilophila wadsworthia
Escherichia coli
Bacteroides dorei/vulgatus
Bacteroides rodentium/uniformis
Bacteroides cellulosilyticus/fragilis
Gemella sanguinis
Clostridium saudiense/disporicum
Staphylococcus lugdunensis
Veillonella parvula
Veillonella atypica
Staphylococcus epidermidis
Rothia mucilaginosa
Veillonella rogosae
Gemella haemolysans
Haemophilus sp.
Streptococcus sp.
Unclassified
Unclassified
Unclassified
Veillonella dispar
Haemophilus influenzae/parainfluenzae
Streptococcus sp.
Streptococcus pseudopneumoniae/infantis
Streptococcus oralis/pseudopneumoniae
Streptococcus sp.
Unclassified
Streptococcus sp. F0442
Streptococcus parasanguinis
Streptococcus sp.
Streptococcus australis
Streptococcus sp.
Component 1
D
Actinobacteria sp.
Actinomyces sp. ICM47
Streptococcus peroris
Streptococcus sp. 263_SSPC
Streptococcus sp.
Streptococcus sp.
Streptococcus sp.
Gemella sanguinis
Rothia mucilaginosa
Unclassified
Veillonella dispar
Rothia mucilaginosa
Bifidobacterium bifidum
Lactobacillus fermentum/oris
Unclassified
Streptococcus parasanguinis
Haemophilus sp.
Veillonella atypica
Gemella haemolysans
Streptococcus oralis/pseudopneumoniae
Streptococcus pseudopneumoniae/infantis
Streptococcus salivarius
Bacteroides cellulosilyticus/fragilis
Enterococcus gallinarum/saccharolyticus
Clostridioides difficile
Bacteroides caccae
Unclassified
Intestinibacter bartlettii
Erysipelatoclostridium ramosum
Unclassified
Unclassified
Eggerthella lenta
Firmicutes sp.
Tyzzerella nexilis
Blautia obeum/wexlerae
Flavonifractor plautii
Flavonifractor plautii
Component 2
E
Bacteroides dorei/vulgatus
Parabacteroides distasonis
Bifidobacterium longum
Escherichia coli
Bacteroides rodentium/uniformis
Bacteroides faecis/thetaiotaomicron
Collinsella aerofaciens
Parabacteroides merdae
Bifidobacterium adolescentis
Bacteroides sp.
Bifidobacterium ruminantium
Bifidobacterium catenulatum/kashiwanohense
Bacteroides cellulosilyticus/fragilis
Bacteroides stercoris
Bifidobacterium pseudocatenulatum
Sutterella wadsworthensis
Unclassified
Bacteroides caccae
Bacteroides caecimuris
Eggerthella lenta
Bifidobacterium bifidum
Streptococcus thermophilus
Clostridium saudiense/disporicum
Actinobacteria sp.
Rothia mucilaginosa
Streptococcus sp.
Unclassified
Unclassified
Klebsiella michiganensis/oxytoca
Streptococcus sp.
Staphylococcus epidermidis
Enterobacter sp.
Haemophilus influenzae/parainfluenzae
Veillonella atypica
Streptococcus parasanguinis
Streptococcus sp.
Enterococcus faecalis
Veillonella parvula
Clostridium perfringens
Unclassified
Veillonella dispar
Veillonella rogosae
Component 3

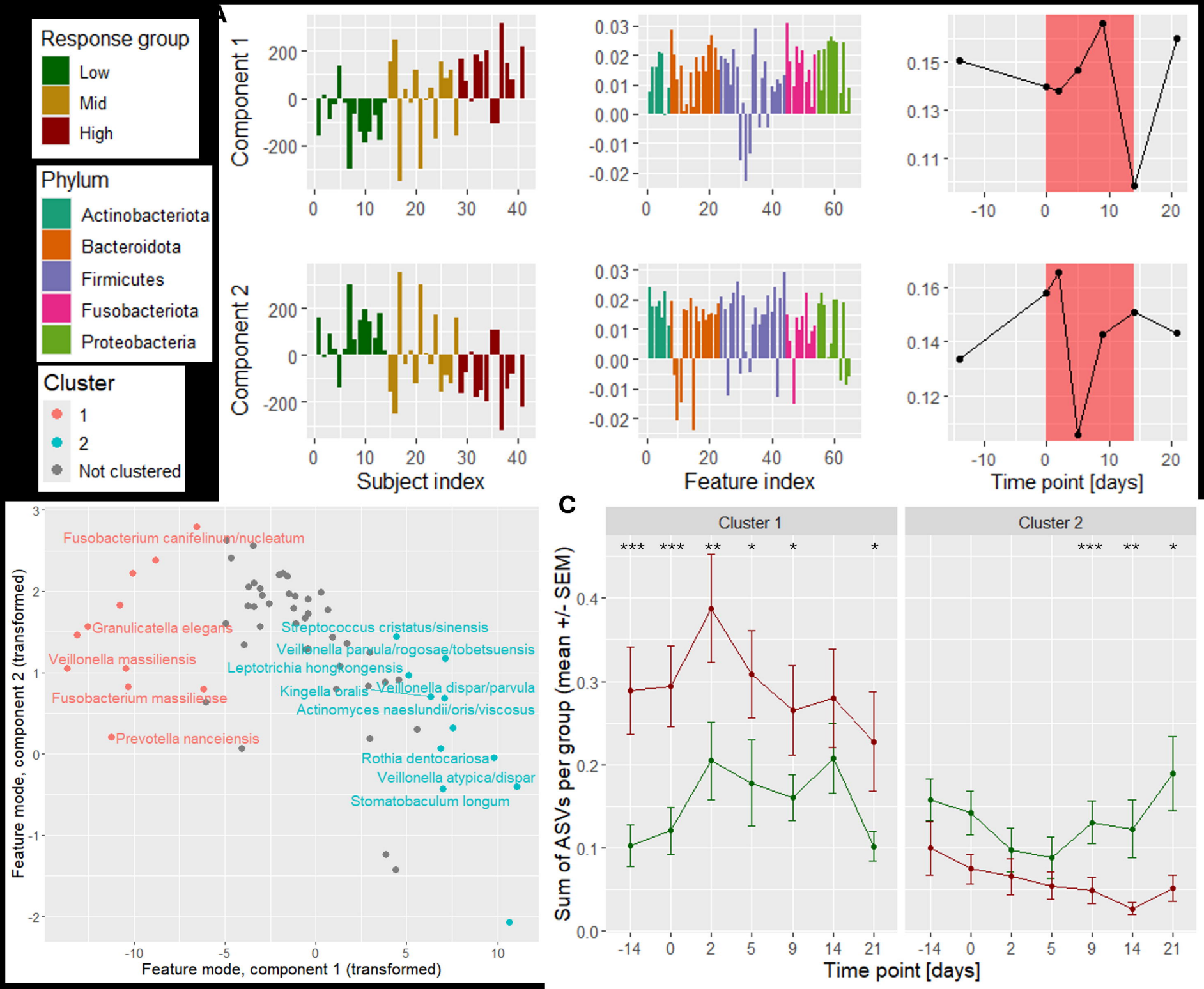
Response group
Low
Mid
High
Phylum
Actinobacteriota
Bacteroidota
Firmicutes
Fusobacteriota
Proteobacteria
Cluster
1
2
Not clustered
A
Component 1
Component 2
Subject index
Feature index
Time point [days]
Fusobacterium canifelinum/nucleatum
Granulicatella elegans
Veillonella massiliensis
Fusobacterium massiliense
Prevotella nanceiensis
Streptococcus cristatus/sinensis
Veillonella parvula/rogosae/tobetsuensis
Leptotrichia hongkongensis
Kingella oralis
Veillonella dispar/parvula
Actinomyces naeslundii/oris/viscosus
Rothia dentocariosa
Veillonella atypica/dispar
Stomatobaculum longum
Feature mode, component 2 (transformed)
Feature mode, component 1 (transformed)
C
Cluster 1
Cluster 2
Sum of ASVs per group (mean +/- SEM)
Time point [days]